

Transport properties of an electron-hole bilayer/superconductor hybrid junction

D. Bercioux,^{1,2,*} T.M. Klapwijk,³ and F. S. Bergeret^{1,4,†}

¹Donostia International Physics Center (DIPC),

Manuel de Lardizbal 4, E-20018 San Sebastián, Spain

²IKERBASQUE, Basque Foundation of Science, 48011 Bilbao, Basque Country, Spain

³Kavli Institute of Nanoscience Delft University of Technology

⁴Centro de Física de Materiales (CFM-MPC) Centro Mixto CSIC-UPV/EHU,
20018 Donostia-San Sebastian, Basque Country, Spain

We investigate the transport properties of a junction consisting of an electron-hole bilayer in contact with normal and superconducting leads. The electron-hole bilayer is considered as a semi-metal with two electronic bands. We assume that in the region between the contacts the system hosts an exciton condensate described by a BCS-like model with a gap Γ in the quasiparticle density of states. We first discuss how the subgap electronic transport through the junction is mainly governed by the interplay between two kinds of reflection processes at the interfaces: The standard Andreev reflection at the interface between the superconductor and the exciton condensate, and a coherent crossed reflection at the semi-metal/exciton-condensate interface that converts electrons from one layer into the other. We show that the differential conductance of the junction shows a minimum at voltages of the order of Γ/e . Such a minimum can be seen as a direct hallmark of the existence of the gapped excitonic state.

PACS numbers: 74.45.+c, 71.35.-y, 73.20.Mf

Introduction.— Semimetals (SMs) could undergo at sufficiently low temperatures, a phase transition into an insulating state described by electron-hole bound pairs. These pairs form a so-called exciton condensate (EC), as theoretically predicted a long time ago, [1–3] and one refers to the system being in an excitonic insulating phase. The ground state of such a phase can be described with the help of a BCS-like theory, in analogy to the superconducting phase. However, the coupling strength in an excitonic insulator is expected to be even weaker than in a superconductor (S). Furthermore, electron-hole recombination can be quite fast, thereby preventing the formation of the condensate. For these reasons the EC remains an elusive phase of matter [1, 2, 4]. Possible SM candidates suggested to undergo a transition to the excitonic insulating phase with an EC are transition-metal dichalcogenide TiSe₂ [5, 6] and HgTe QWs with a thickness of 20 nm [7–9]. However, there is no conclusive evidence for an EC in such systems. So far the most successful attempt to obtain an EC is based on the condensation of excitons coupled to light confined within CdTe/CdMgTe micro-cavities — the so-called exciton-polaritons [10].

Besides bulk semi-metals, there have been several proposals to create an EC in systems with spatially separated electron and hole gases in order to reduce the electron-hole recombination rate. The exciton formation in such electron-hole bilayers can be detected by Coulomb drag measurements [11–16]. According to the theory, if the excitons form a condensate one expects a discontinuity in the drag at the critical temperature and a divergence when $T \rightarrow 0$ [17]. Although certain anomalies of the Coulomb drag as a function of temperature have been observed [11, 12], it is hard to attribute them to the

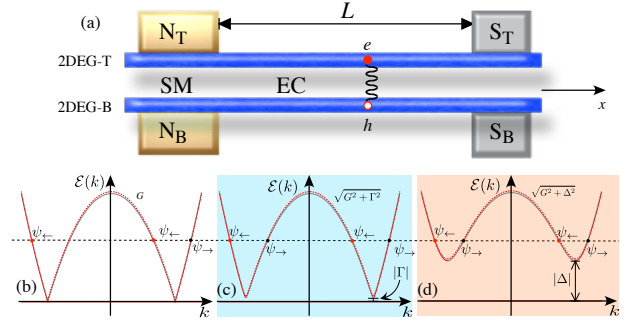


FIG. 1: (a) Sketch of the electron-hole bilayer with the two normal ($N_{T/B}$) and two superconducting electrodes ($S_{T/B}$), the EC region in the middle has length L . Energy spectra for the SM region (b), the EC region (c), and SSM one (d).

formation of an exciton condensate.

The primary motivation of this Letter is to propose and explore an additional type of measurements to validate the existence of an EC in electron-hole bilayers. Instead of measuring the Coulomb drag, we suggest to perform a differential conductance measurement using normal and superconducting electrodes (see Fig. 1), so to directly unveil the presence of the excitonic gap. We show that the transport at low voltages is determined by the competition between the intra-layer Andreev reflection and the inter-layer normal reflection between the SM and the EC parts of the system. The latter process is analogous to the one introduced by Rontani and Sham for direct SM/EC interfaces [18–20]. We discuss the competition between these two type of reflections as a function of the length of the EC region and show that this competition leads to a minimum of the full differential conductance

at a voltage V_0 of the order of the EC order parameter.

Model and Formalism.— We consider an ideal two-dimensional electron-hole bilayer, characterized by two parallel two-dimensional electron gases with opposite particle filling, as illustrated in Fig. 1(a) — the top layer (TL) is “electron-doped” whereas the bottom layer (BL) is “hole-doped”. By gating the two layers independently it is possible to modulate the band overlap G between the bands of the TL/BL [21]. We assume a spatial modulation along the x -axes of the Coulomb interaction in the electron-hole bilayer. In the parts of the bilayer covered by the metallic electrodes, the charge screening allows neglecting the Coulomb interaction. Thus the left and right parts of the system, are described by a SM consisting of two bands — one from each layer — crossing at the Fermi level [see Fig. 1(a)]. Due to the proximity effect, we assume an induced superconducting gap Δ on the part of the layers below the S contacts [see Fig. 1(c)]. In the region between the contacts the reduced screening results in an *indirect* EC described by the order parameter Γ [21] [see Fig. 1(b)].

To be precise, the structure shown in Fig. 1(a) is modelled as a SM, *i.e.*, $\Gamma = \Delta = 0$, in contact with a central region of length L with a finite EC coupling ($\Gamma \neq 0$ and $\Delta \neq 0$). In the region $x > L$ we assume $\Delta \neq 0$ due to the proximity from the S electrodes [22] and $\Gamma = 0$. We denote this region as SSM. This junction is described by the following Hamiltonian written in an extended Nambu space [23]:

$$\mathcal{H}_{\text{Hyb}} = \begin{pmatrix} \frac{\mathbf{p}^2}{2m} - G & \Gamma(x) & \Delta(x)e^{i\phi} & 0 \\ \Gamma(x)^* & G - \frac{\mathbf{p}^2}{2m} & 0 & \Delta(x)e^{i\phi} \\ \Delta(x)e^{-i\phi} & 0 & G - \frac{\mathbf{p}^2}{2m} & -\Gamma(x) \\ 0 & \Delta(x)e^{-i\phi} & -\Gamma(x)^* & \frac{\mathbf{p}^2}{2m} - G \end{pmatrix}, \quad (1)$$

where

$$\Gamma(x) = \Gamma\Theta(x)(1 - \Theta(x - L)), \quad (2a)$$

$$\Delta(x) = \Delta\Theta(x - L), \quad (2b)$$

and $\Theta(x)$ is the Heaviside step function. The Hamiltonian (1) is written in the basis defined by the *bi*-spinor $\Psi = (\psi_{\text{TL},\sigma}, \psi_{\text{BL},\sigma}, \psi_{\text{TL},-\sigma}^\dagger, \psi_{\text{BL},-\sigma}^\dagger)$, where σ is the spin [23, 24]. We account for possible elastic reflection at the SM/EC and EC/SSM interfaces by introducing delta-barriers in the system Hamiltonian [25], $\mathcal{H}_{\text{int}} = H_{\text{SM/EC}}\delta(x) + H_{\text{EC/SSM}}\delta(x - L)$. This reflection can be ascribed, for example, to the mismatch of the Fermi wave vector in the different regions [26].

We analyse the scattering properties of this hybrid SM/EC/SSM junction by matching the scattering states at each interface separating these three regions [27]. In the SM region, there is no coupling between the TL and BL nor between electron/hole of the same layer. Thus, we can consider an electron (hole) in the TL (BL) as an

initial scattering state. In the middle, EC, region, there is a finite coupling between electrons of TL and BL proportional to Γ . And in the SSM region the superconducting pairing Δ couples electrons and holes within the same layer.

We summarize all possible processes that an incoming electron from the TL of the SM at energies smaller than Γ and Δ , may experience. If we look at the SM/EC interface the electron can be either normal reflected in the same layer with amplitude $-r_{\text{N,T} \rightarrow \text{T}} \equiv r_{\text{NTT}}$, or in the opposite layer $-r_{\text{N,T} \rightarrow \text{B}} \equiv r_{\text{NTB}}$. The latter process resembles the Andreev reflection at the S/N interface and was studied by Rontani and Sham in Ref. [18–20]. It results in an exciton in the EC region. Whereas at the EC/SSM interface the electron can be Andreev-reflected into a hole either in the same layer $-r_{\text{A,T} \rightarrow \text{T}} \equiv r_{\text{ATT}}$, or into the other layer $-r_{\text{A,T} \rightarrow \text{B}} \equiv r_{\text{ATB}}$. It is interesting to notice that the reflection amplitude r_{ATB} is the analog to the Andreev specular-reflection in Dirac-material/superconductor hybrid junctions [22].

For energies higher than the EC gap, $\mathcal{E} > |\Gamma|$, the particles travel through the EC region as propagating waves. In contrast, for $\mathcal{E} < |\Gamma|$, the quasi-bound states are characterized by complex momenta describing evanescent modes. The characteristic decay length of these modes ξ_Γ , is energy dependent and given by:

$$\xi_\Gamma^{-1} = \sqrt{\frac{1}{2} \left(\chi_Q + \sqrt{\chi_Q^2 + \frac{4m^2}{\hbar^4} (\Gamma^2 - \mathcal{E}^2)} \right)}. \quad (3)$$

where $\chi_Q = Q^2 - \frac{2mG}{\hbar^2}$, here Q is the momentum parallel to the interfaces that is conserved in the scattering process [27]. When the band overlap G is the dominant energy scale, *i.e.*, $G \gg \max[\Gamma, \Delta, \mathcal{E}]$, the EC characteristic length scale is approximated by

$$\xi_\Gamma = \frac{4\hbar\sqrt{mG^3}}{\Gamma(4mG + Q^2\hbar^2)}. \quad (4)$$

In what follows, we focus on the subgap transport, *i.e.* we consider the injection of electrons from the TL with energies smaller than the SSM gap, $\mathcal{E} < |\Delta|$. Furthermore, we also assume that $\Gamma < \Delta < G$. The probability for the four possible reflection channels in the SM electrode are then given by [27]:

$$R_{\text{NTT}}(\alpha) = |r_{\text{NTT}}(\alpha)|^2, \quad (5a)$$

$$R_{\text{NTB}}(\alpha) = |r_{\text{NTB}}(\alpha)|^2 \left| \frac{\text{Im}[\kappa_-]}{\kappa_+}(\alpha) \right| \Theta(G - \mathcal{E}), \quad (5b)$$

$$R_{\text{ATT}}(\alpha) = |r_{\text{ATT}}(\alpha)|^2 \left| \frac{\text{Im}[\kappa_-]}{\kappa_+}(\alpha) \right| \Theta(G - \mathcal{E}), \quad (5c)$$

$$R_{\text{ATB}}(\alpha) = |r_{\text{ATB}}(\alpha)|^2, \quad (5d)$$

where α is the injection angle. For angles larger than a critical $\alpha_c = \arcsin[\pm\sqrt{|G - \mathcal{E}|/(\mathcal{E} + G)}]$, $R_{\text{NTB}} =$

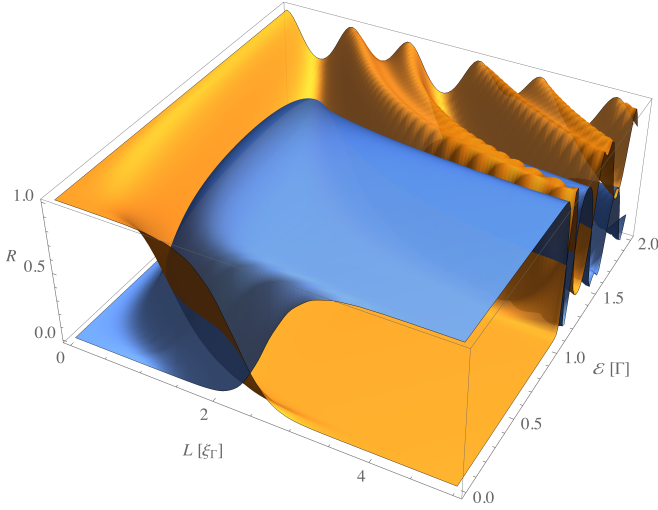


FIG. 2: R_{NTB} reflection (blue surface) and R_{ATT} (orange surface) reflection as a function of the length of EC region L and injection energy \mathcal{E} , both surfaces are shown for injection energies up to Δ . Here, we have used $\Gamma = 1$, $\Delta = 2\Gamma$, $G = 100\Gamma$, and normal incidence $\alpha = 0$.

$R_{ATT} = 0$ because of the lack of propagating states on the TL/BL. The actual form of the reflection and transmissions amplitudes are obtained by solving the scattering problem at the two interfaces [27].

Results.— We now analyze the dependence of the probabilities (5) on the length of the EC region. In the limiting case $L = 0$ the system consists of a simple SM/SSM junction. In this case, the absence of the EC leads to $r_{NTB} = 0$. Moreover, r_{ATB} also vanishes and the results for a clean interface coincide with the standard N/S junction case [25, 27]. Here we stress the analogy between the interlayer Andreev reflection and the specular Andreev reflection typical of SM with Dirac spectrum again [22, 28, 29]. If there is no EC then electrons from the TL and BL are decoupled, and hence all reflections occur within the same layer only.

We now focus on the more interesting case of a finite EC region, $L \neq 0$. In Fig. 2 we present the reflections R_{NTB} and R_{ATT} as a function of the injection energy and length of the EC region for a normal injection angle ($\alpha = 0$). For a length smaller than ξ_Γ , the probability for an injected electron in the TL to reach the EC/SSM interface is large. The electron is then Andreev reflected as a hole of the same layer. This explains that for small L , the Andreev reflection, R_{ATT} , dominates over the interlayer one, R_{NTB} , at all energies.

By increasing the length of the EC region, the probability to reach the EC/SSM interface, for an injected electron with energy $\mathcal{E} < \Gamma$ decreases and hence the R_{ATT} processes are suppressed, whereas the R_{NTB} ones are enhanced. The crossover between these two behaviors depends on the injection energy. In the limiting case

$L \gg \xi_\Gamma$ the probability for the injected TL electron of reaching the SSM electrode is exponentially small and the system behaves as a SM/EC junction with the reflection probability $R_{NTB} = 1$ [18, 19]. For injection energies larger than the EC gap $|\Gamma|$ (but smaller than Δ), all electrons propagate towards the EC/SSM interface and hence Andreev processes dominate, whereas R_{NTB} decreases to zero by increasing the injection energy. The oscillatory behavior we observe for this energy range is a feature of quasi-bound states in the EC region.

Analytically we can calculate the reflection probabilities (5b) and (5c) in the short-junction limit, $\delta = L/\xi_\Gamma \ll 1$ within the Andreev approximation, *i.e.* $G \gg \text{Max}[\mathcal{E}, \Delta, \Gamma]$. In this limits and for zero injection angle $\alpha = 0$, we obtain

$$R_{NTB} = 4\delta^2 \frac{\mathcal{E}^2 \Gamma^2}{\Delta^2 (\Gamma^2 - \mathcal{E}^2)}, \quad (6a)$$

$$R_{ATT} = 1 - 4\delta^2 \frac{\mathcal{E}^2 \Gamma^2}{\Delta^2 (\Gamma^2 - \mathcal{E}^2)}, \quad (6b)$$

$$R_{NTT} = 0. \quad (6c)$$

These expressions are in agreement with the numerical results shown in Fig. 2 within the small L region. Notice that for the large value of G chosen, $G = 100\Gamma$, the probability for the reflection R_{ATB} is negligibly small. However, if one choose a smaller G and a larger injection angle α , R_{ATB} is finite [27]. In this latter case both types of Andreev reflections, R_{ATB} and R_{ATT} , may take place simultaneously. This differs from the case of retro- and specular-Andreev reflections in SM with Dirac spectrum, where one or the other is finite by crossing the charge neutrality point [22, 28, 29].

To make a connection with possible transport experiments, we now turn the focus upon the differential conductance (DC), which is a quantity accessible in conventional transport experiments. For this purpose, we assume that the two left normal contacts are placed at the same potential V and that the two right superconducting contacts are grounded. The DC can be expressed in terms of the reflection probabilities (5), by using a generalized expression based on the Blonder-Tinkham-Klapwijk formula [25, 30],

$$\frac{\partial I}{\partial V} = G_0(eV) \int_0^{\frac{\pi}{2}} \sum_{\beta \in \{T, B\}} \left[1 - R_{NT\beta}(eV, \alpha) + R_{AT\beta}(eV, \alpha) \right] \cos \alpha d\alpha. \quad (7)$$

Here $G_0(eV)$ is the differential conductance of the normal state.

Figure 3(a) shows the DC as a function of the injection energy, which is proportional to the applied voltage, and for different values of the length L . Notice first that the DC is not equal to $2G_0$ for $L = 0$. This is a consequence of considering a finite chemical potential [22]. For a finite

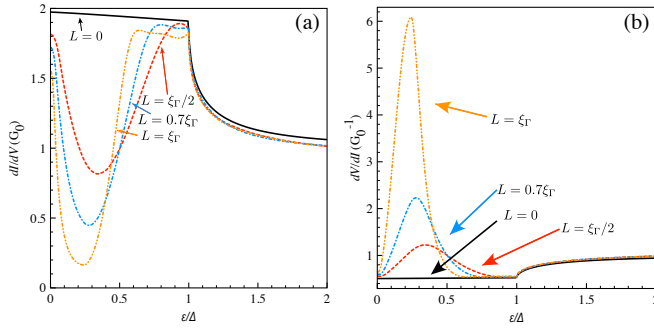


FIG. 3: Panel (a): Differential conductance as a function of the applied bias and for different lengths L of the EC region, the various lines correspond to $\Gamma = 1$, $\Delta = 4\Gamma$, $G = 100\Gamma$ and $H_L = H_R = 0$. Panel (b): Differential resistance as a function of the applied bias and different length of the EC region. In the figure we have set $\Gamma = 1$, $\Delta = 12\Gamma$, $G = 60\Gamma$ and $H_{SM/EC} = H_{EC/SSM} = 0.5$. The parameters are chosen in accordance to Ref. [9, 31]. In both panels The different lines refer to $L = 0$ (black-solid line), $L = \xi_r/2$ (red dashed line), $L = 0.7\xi_r$ (blue dashed-dotted line), and $L = \xi_r$ (orange dashed-dashed-dotted-dotted line).

length EC region the DC decreases faster as a function of the voltage, it reaches a minimum and then increases up to a voltage of the order of Δ . It is also worth to notice that the DC of the normal state in the presence of a finite EC is also smaller compared to the case without it.

The decrease of the DC is due to a normal reflection channel that accounts for electrons injected from the TL and reflected into the BL. Thus, the presence of a finite length EC region entirely accounts for the minimum in the DC. If the length L exceeds the decay length ξ_r , injected electrons with $E < \Gamma$ rarely reach the superconducting electrode (c.f. Fig. 2) and therefore the DC remains small up to voltages of the order $|\Gamma|$ [18].

We can obtain an analytical expression for the low bias behavior of the DC in the short-junction limit, using Eqs. (6), and within the Andreev approximation:

$$\frac{dI}{dV} = G_0 \left[1 - 8\delta^2 \frac{(eV)^2 \Gamma^2}{\Delta^2 (\Gamma^2 - (eV)^2)} \right]. \quad (8)$$

According to this expression the low voltage peak in the DC is of the order of Γ . This suggests that transport measurement using superconducting electrodes could be used to directly estimate the size of the order parameter Γ .

Our results for the differential conductance may help to understand measurements of the differential resistance of a superconductor/HgTe-quantum well junction. The quantum well has a width of 20 nm [9]. One of the most striking findings in this experiment is a zero-bias peak in the measured differential resistance [9] that can be

seen as the manifestation of an EC gap. Indeed, in the light of our model the size of the zero-bias peak corresponds to the EC gap. This comparison is shown in Fig. 3(b) where we plot the differential resistance by choosing parameters consistent with the experiments on HgTe quantum wells [9, 31]. Although the agreement between theory and experiment looks promising we would like to be cautious at this point because our approach assumes a full ballistic system, whereas the samples measured in Ref. [9] have a size of several μm , and disorder might play a role [32]. Further experiments and analysis are needed to draw definite conclusions.

Conclusions.— We have studied the electronic transport through an electron-hole bilayer in contact with normal and superconducting electrodes. We have assumed that the electron-hole bilayer hosts an exciton condensate. The transport properties of this junctions are determined by the competition of different coherent reflection processes occurring at the interfaces with the normal and superconducting electrodes. As a consequence of this competition, the differential conductance has a minimum at voltages of the order Γ/e , where Γ is the EC order parameter. The observation of this minimum in an electron-hole bilayer system represents a unique hallmark of the presence of the EC. Good candidates for our proposal are double bilayer-graphene systems separated by hexagonal boron nitrate [13, 14]. In bilayer-graphene, superconductivity induced by proximity effect has been already observed [28]. Moreover, from our model one might interpret the zero bias-peak observed in the differential resistance of a HgTe quantum well/superconductor junction as a manifestation of an EC phase.

Acknowledgments.— Discussions with B. Bujnowski, E. Deviatov, F. Konschelle, V. Golovach, T. T. Heikkilä, P. Lucignano, M. Rontani and T. van den Berg are acknowledged. The work of DB and FSB is supported by Spanish Ministerio de Economía y Competitividad (MINECO) through the project FIS2014-55987-P and by the Transnational Common Laboratory *Quantum-ChemPhys*. TMK acknowledges the financial support from the European Research Council Advanced grant no. 339306 (METIQUIM), and the Ministry of Education and Science of the Russian Federation, contract N 14.B25.31.0007 of 26 June 2013.

* Electronic address: dario.bercioux@dipc.org

† Electronic address: sebastian.bergeret@ehu.es

- [1] L. V. Keldysh and Y. Kopayev, Fiz. Tverd. Tela **6**, 2791 (1965), [Sov. Phys. Solid State **6**, 2219 (1965)].
- [2] D. Jérôme, T. M. Rice, and W. Kohn, Phys. Rev. **158**, 462 (1967).
- [3] M. Combescot and S.-Y. Shiao, *Excitons and Cooper Pairs: Two Composite Bosons in Many-Body Physics* (Oxford University Press, 2016).

- [4] B. I. Halperin and T. M. Rice, *Rev. Mod. Phys.* **40**, 755 (1968).
- [5] C. Monney, E. F. Schwier, M. G. Garnier, N. Mariotti, C. Didiot, H. Cercellier, J. Marcus, H. Berger, A. N. Titov, H. Beck, et al., *New J. Phys.* **12**, 125019 (2010).
- [6] K. Rossnagel, *J. Phys. Condens. Matter* **23**, 213001 (2011).
- [7] G. M. Minkov, A. V. Germanenko, O. E. Rut, A. A. Sherstobitov, S. A. Dvoretzki, and N. N. Mikhailov, *Phys. Rev. B* **88**, 155306 (2013).
- [8] M. Knap, J. D. Sau, B. I. Halperin, and E. Demler, *Phys. Rev. Lett.* **113**, 186801 (2014).
- [9] A. Kononov, S. V. Egorov, Z. D. Kvon, N. N. Mikhailov, S. A. Dvoretzki, and E. V. Deviatov, *Phys. Rev. B* **93**, 041303 (2016).
- [10] J. Kasprzak, M. Richard, S. Kundermann, A. Baas, P. Jeambrun, J. M. J. Keeling, F. M. Marchetti, M. H. Szymańska, R. André, J. L. Staehli, et al., *Nature* **443**, 409 (2006).
- [11] A. F. Croxall, K. Das Gupta, C. A. Nicoll, M. Thangaraj, H. E. Beere, I. Farrer, D. A. Ritchie, and M. Pepper, *Phys. Rev. Lett.* **101**, 246801 (2008).
- [12] J. A. Seamons, C. P. Morath, J. L. Reno, and M. P. Lilly, *Phys. Rev. Lett.* **102**, 026804 (2009).
- [13] J. I. A. Li, T. Taniguchi, K. Watanabe, J. Hone, A. Levchenko, and C. R. Dean, *Phys. Rev. Lett.* **117**, 046802 (2016).
- [14] K. Lee, J. Xue, D. C. Dillen, K. Watanabe, T. Taniguchi, and E. Tutuc, *Phys. Rev. Lett.* **117**, 046803 (2016).
- [15] M. M. Fogler, L. V. Butov, and K. S. Novoselov, *Nat. Commun.* **5**, 521 (2014).
- [16] E. V. Calman, C. J. Dorow, M. M. Fogler, L. V. Butov, S. Hu, A. Mishchenko, and A. K. Geim, *Appl. Phys. Lett.* **108**, 101901 (2016).
- [17] G. Vignale and A. H. Macdonald, *Phys. Rev. Lett.* **76**, 2786 (1996).
- [18] M. Rontani and L. J. Sham, *Solid State Commun.* **134**, 89 (2005).
- [19] M. Rontani and L. J. Sham, *Phys. Rev. Lett.* **94**, 186404 (2005).
- [20] B. Wang, J. Peng, D. Y. Xing, and J. Wang, *Phys. Rev. Lett.* **95**, 086608 (2005).
- [21] X. Zhu, P. B. Littlewood, M. S. Hybertsen, and T. M. Rice, *Phys. Rev. Lett.* **74**, 1633 (1995).
- [22] C. Beenakker, *Phys. Rev. Lett.* **97**, 067007 (2006).
- [23] F. Dolcini, D. Rainis, F. Taddei, M. Polini, R. Fazio, and A. H. Macdonald, *Phys. Rev. Lett.* **104**, 027004 (2010).
- [24] S. Peotta, M. Gibertini, F. Dolcini, F. Taddei, M. Polini, L. B. Ioffe, R. Fazio, and A. H. Macdonald, *Phys. Rev. B* **84**, 184528 (2011).
- [25] G. E. Blonder, M. Tinkham, and T. M. Klapwijk, *Phys. Rev. B* **25**, 4515 (1982).
- [26] The use of the BTK formalism assumes a sharp boundary between the different regions. In particular, an abrupt change of the superconducting pair correlations at the SSM/EC interface. This assumption is well justified if the size of the contact between the two regions is much smaller than its lateral dimensions. This condition can be achieved experimentally by proper design of the contact. However, even in the case of a smooth transition of the pair correlations at the interface, we expect to have qualitatively similar results.
- [27] See Supplemental Material (Supp. Mat.) [url] for full details of the calculations, which includes Ref. [33].
- [28] D. K. Efetov, L. Wang, C. Handschin, K. B. Efetov, and J. Shuang, *Nat. Phys.* **12**, 328 (2015).
- [29] W. Chen, L. Jiang, R. Shen, L. Sheng, B. G. Wang, and D. Y. Xing, *EPL* **103**, 27006 (2013).
- [30] N. A. Mortensen, K. Flensberg, and A.-P. Jauho, *Phys. Rev. B* **59**, 10176 (1999).
- [31] Z. D. Kvon, E. B. Olshanetsky, E. G. Novik, D. A. Kozlov, N. N. Mikhailov, I. O. Parm, and S. A. Dvoretzki, *Phys. Rev. B* **83**, 193304 (2011).
- [32] A more detailed comparison of our results with those of the experiment of Ref. [9] is given in the Supplementary Material.
- [33] D. Averin and A. Bardas, *Phys. Rev. Lett.* **75**, 1931 (1995).

The scattering states

In this section we briefly introduce the scattering states in the three regions of the electron-hole bilayer system we have considered in the main text, this is constituted by a SM region on the left, an EC region of length L in the center and a superconducting region on the right. The scattering states in the SM region read:

$$\psi_{\text{SM}} = e^{iQy} \left\{ [e^{i\kappa+x} + r_{\text{NTT}} e^{-i\kappa+x}] \begin{pmatrix} 1 \\ 0 \\ 0 \\ 0 \end{pmatrix} + r_{\text{NTB}} e^{i\kappa-x} \begin{pmatrix} 0 \\ 1 \\ 0 \\ 0 \end{pmatrix} + r_{\text{ATT}} e^{i\kappa-x} \begin{pmatrix} 0 \\ 0 \\ 1 \\ 0 \end{pmatrix} + r_{\text{ATB}} e^{-i\kappa+x} \begin{pmatrix} 0 \\ 0 \\ 0 \\ 1 \end{pmatrix} \right\}, \quad (9)$$

here Q is the component of the momentum along the y direction. Being that we consider a translational invariant interface between the three regions, the component of the momentum parallel to this interface is a conserved quantity in the overall scattering process. At a fixed injection energy \mathcal{E} , the momenta κ_{\pm} are expressed by the following relations [c.f. Fig. 1(b) main text]:

$$\kappa_{\pm} = \sqrt{\frac{2m}{\hbar^2} (G \pm \mathcal{E}) - Q^2}. \quad (10)$$

In the SSM region, the superconducting pairing couples electrons and holes of the same layer, but there is no direct coupling between electrons of the two layers. The incoming electron from the SM region can be transmitted as quasi-electron or quasi-hole either in the top later (TL) (t_{QET} and t_{QHT}) or bottom layer (BL) (t_{QEB} and

t_{QHB}). The transmitted wave function reads:

$$\psi_{\text{SSM}} = e^{iQy} \left[t_{\text{QET}} e^{ik+x} \begin{pmatrix} u_{\text{T}} \\ 0 \\ v_{\text{T}} e^{i\phi} \\ 0 \end{pmatrix} + t_{\text{QHT}} e^{-ik-x} \begin{pmatrix} v_{\text{T}} \\ 0 \\ u_{\text{T}} e^{i\phi} \\ 0 \end{pmatrix} + t_{\text{QHB}} e^{ik+x} \begin{pmatrix} 0 \\ u_{\text{B}} \\ 0 \\ v_{\text{B}} e^{i\phi} \end{pmatrix} + t_{\text{QEB}} e^{-ik-x} \begin{pmatrix} 0 \\ v_{\text{B}} \\ 0 \\ u_{\text{B}} e^{i\phi} \end{pmatrix} \right]. \quad (11)$$

The momenta in the SSM [c.f. Fig. 1(d) main text] region are

$$k_{\pm} = \sqrt{\frac{2m}{\hbar^2} (G \pm \sqrt{\mathcal{E}^2 - \Delta^2}) - Q^2}. \quad (12)$$

The coherence factor are the $u_{\text{T/B}}$ and $v_{\text{T/B}}$ are the standard one of a s -wave superconductor, here T/B is for TL and BL, respectively. Note that there is change of sign between two layers, this is due to their opposite curvature of the energy dispersion:

$$u_{\text{T/B}} = \sqrt{\frac{1}{2} \pm \sqrt{1 - \left(\frac{\Delta}{\mathcal{E}}\right)^2}} \quad (13a)$$

$$v_{\text{T/B}} = \sqrt{\frac{1}{2} \mp \sqrt{1 - \left(\frac{\Delta}{\mathcal{E}}\right)^2}} \quad (13b)$$

In the middle EC region, there is a finite Coulomb coupling in the electron-hole bilayer. Here the wave function is given by counter-propagating states for the four possible states: quasi-electron/hole in TL/BL:

$$\psi_{\text{EC}}(x) = e^{iQy} \left\{ (a_1 e^{iq+x} + c_1 e^{-iq+x}) \begin{pmatrix} u_e \\ v_e e^{-ix} \\ 0 \\ 0 \end{pmatrix} + (b_1 e^{-iq-x} + d_1 e^{iq-x}) \begin{pmatrix} v_e \\ u_e e^{-ix} \\ 0 \\ 0 \end{pmatrix} + (a_2 e^{iq+x} + c_2 e^{-iq+x}) \begin{pmatrix} 0 \\ 0 \\ v_h \\ u_h e^{-ix} \end{pmatrix} + (b_2 e^{-iq-x} + d_2 e^{iq-x}) \begin{pmatrix} 0 \\ 0 \\ u_h \\ v_h e^{-ix} \end{pmatrix} \right\}. \quad (14)$$

The momenta in EC region [c.f. Fig. 1(c) main text] are defined as:

$$q_{\pm} = \sqrt{\frac{2m}{\hbar^2} (G \pm \sqrt{\mathcal{E}^2 - \Gamma^2}) - Q^2}. \quad (15)$$

For this case the the coherent function are very similar

to the superconducting one, they are here given by: [18]

$$u_{e/h} = \sqrt{\frac{1}{2} + \sqrt{1 - \left(\frac{\Gamma}{\mathcal{E}}\right)^2}} \quad (16a)$$

$$v_{e/h} = \sqrt{\frac{1}{2} - \sqrt{1 - \left(\frac{\Gamma}{\mathcal{E}}\right)^2}} \quad (16b)$$

The density plot of the four reflection channels are presented in S-Fig. 4 for the case of large and small band overlap G . It can be observed that for small injection angle φ the R_{NTB} and the R_{ATT} reflection are the dominant processes, on the other side at large angles the R_{NTT} and

R_{ATB} reflection are finite, but smaller than R_{NTB} and R_{ATT} .

The boundary conditions

The scattering amplitudes of the various scattering processes can be obtained by imposing the continuity of the wave function in $x = 0$ and $x = L$:

$$\psi_{\text{SM}}(0^-) = \psi_{\text{EC}}(0^+) \quad (17a)$$

$$\psi_{\text{EC}}(L^-) = \psi_{\text{SSM}}(L^+) \quad (17b)$$

the continuity of the first derivative in the same points. When considering a possible mismatch of the Fermi velocity at the interface between the various region, we can model this via delta-barriers of strength $H_{\text{SM/EC}}$ in $x = 0$ and $H_{\text{EC/SSM}}$ in $x = L$. [25] In this case the first derivative has a jump that is opposite for the TL and BL [18]:

$$\psi'_{\text{EC}}(0^+) - \psi'_{\text{SM}}(0^-) = \frac{2mH_{\text{SM/EC}}}{\hbar^2} S_z \psi_{\text{SM}}(0) \quad (18a)$$

$$\psi'_{\text{SSM}}(L^+) - \psi'_{\text{EC}}(L^-) = \frac{2mH_{\text{EC/SSM}}}{\hbar^2} S_z \psi_{\text{EC}}(L). \quad (18b)$$

where we have introduced the boundary matrix S_z defined as:

$$S_z = \mathbb{I}_2 \otimes \sigma_z = \begin{pmatrix} 1 & 0 & 0 & 0 \\ 0 & -1 & 0 & 0 \\ 0 & 0 & 1 & 0 \\ 0 & 0 & 0 & -1 \end{pmatrix}. \quad (19)$$

The critical angle α_c

Using simple kinematic consideration we can determine the expression for the critical angle α_c Eq. (4) of the main text. We need only to account for the conservation of the momentum parallel to the interface $k_y = Q$. For each of the layer involved in the transport mechanism, momenta in polar coordinate read (see S-Fig. 5):

$$k_{\beta,x} = \kappa_\beta \cos \alpha_{\text{in}} \quad (20a)$$

$$k_{\beta,y} = \kappa_\beta \sin \alpha_{\text{in}} \quad (20b)$$

$$(20c)$$

with $\beta \in \{\text{TL}, \text{BL}\}$. The moduli are expressed by

$$\kappa_{\text{TL}} = \sqrt{\frac{2m(\mathcal{E} + G)^2}{\hbar}} \quad (20d)$$

$$\kappa_{\text{BL}} = \sqrt{\frac{2m(G - \mathcal{E})^2}{\hbar}}. \quad (20e)$$

The normal reflection inside the same layer has a propagation direction opposite to the incoming one, the same

is true for electrons that are converted into electrons of the BL. For electrons injected from the TL and converted into holes of the TL or converted into holes of the BL, the reflection angle is given by:

$$\alpha_{\text{NTB}}^{\text{ATT}} = \arcsin \left[\frac{\hbar Q}{\sqrt{2m(G - \mathcal{E})}} \right], \quad (21)$$

for injection energies \mathcal{E} exceeding the band overlap G , the angle is becoming complex and the corresponding mode becomes evanescent. By imposing $2m/\hbar^2(G - \mathcal{E}) - Q^2 \leq 0$ we can determine the critical injection angle α_c :

$$\alpha_c = \arcsin \left[\sqrt{\frac{|G - \mathcal{E}|}{G + \mathcal{E}}} \right]. \quad (22)$$

Case of a EC region of zero length

Here we will presents the results in the case the length of the EC region is zero. This corresponds to a lack of a region where carriers of the electron-hole bilayer are coupled. Thus, the hybrid junction reduced to a SM place in contact with a proximized SM. This corresponds to solve the matching problem with wave function (9) and (11). In the case of the scattering state (9), we are considering an initial incoming electron in the TL. Using this initial incoming state, the amplitudes for reflection process read:

$$r_{\text{ATT}} = \frac{u_{\text{T}} v_{\text{T}} e^{-i\phi}}{\gamma} \quad (23a)$$

$$r_{\text{NTB}} = 0 \quad (23b)$$

$$r_{\text{NTT}} = -\frac{Z(Z - i)(u_{\text{T}} - v_{\text{T}})(u_{\text{T}} + v_{\text{T}})}{\gamma} \quad (23c)$$

$$r_{\text{ATB}} = 0, \quad (23d)$$

whereas for transmissions read:

$$t_{\text{QET}} = \frac{u_{\text{T}} + i u_{\text{T}} Z}{\gamma} \quad (24a)$$

$$t_{\text{QEB}} = 0 \quad (24b)$$

$$t_{\text{QHT}} = \frac{i v_{\text{T}} Z}{\gamma} \quad (24c)$$

$$t_{\text{QHB}} = 0, \quad (24d)$$

here $t_{\text{QET/QHT}}$ is the transmission as the quasi-electron/quasi-hole in the TL, whereas $t_{\text{QEB/QHB}}$ is the transmission as the quasi-electron/quasi-hole in the BL. For both sets of reflection and transmission we have introduced the factor:

$$\gamma = u_{\text{T}}^2 + Z^2(u_{\text{T}} - v_{\text{T}})(u_{\text{T}} + v_{\text{T}})$$

Here $Z = 2mH_{\text{int}}/\hbar^2$ is the dimensionless strength of the delta barrier at the SM/S interface. Importantly, all the

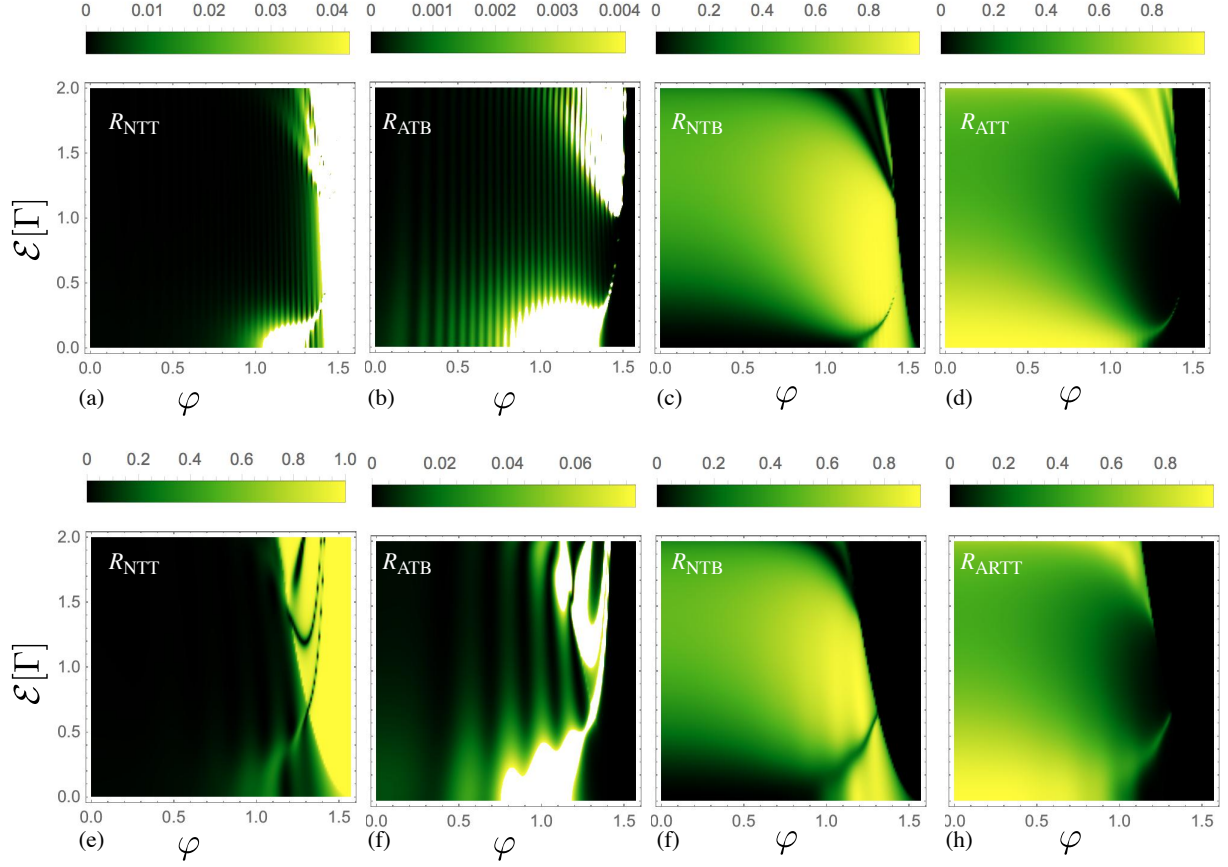


FIG. 4: The four reflection channels as a function of injection angle φ and injection energy \mathcal{E} . Panels (a) to (d), we have set the band overlap to $G = 100$, whereas in Panels (e) to (h) we have $G = 20$. In all Panels $\Gamma = 1$, $\Delta = 2\Gamma$ and $L = \xi_\Gamma$.

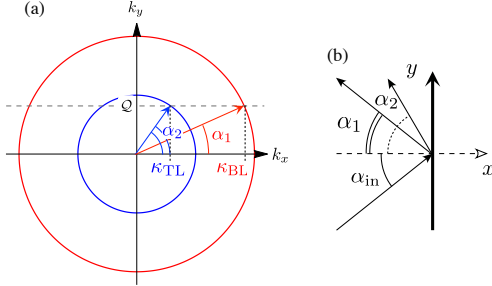


FIG. 5: Panel (a): The two circle corresponding to the Fermi surface for the top (in red) and the bottom (in blue) layer. The momenta along the y -axis Q is conserved in the scattering process, this produce reflection angles for normal reflection in the TL and for hole reflection in the BL α_1 , this is opposite to the incoming one α_{in} . For the case of normal reflection in the BL and hole reflection in the TL, the reflection angle is α_2 . Panel (b): a sketch of the reflection angles with respect to the incoming one α_{in} .

interlayer crossing processes have zero probability amplitudes. In the limit of $Z \rightarrow 0$ we recover the standard results for S/N junctions. [25] Starting with a different

initial scattering state, *e.g.*, an hole in the BL, we get expressions similar to Eqs. (23)-(24) but still without a direct process between TL and BL.

Analytical results

In this appendix we show how to get the analytical results (6a)-(6b) of the main text. Both results are obtained assuming that the band overlap is the dominant energy scale $G \gg \max[\mathcal{E}, \Gamma, \Delta]$ — as the standard *Andreev-like* approximation in superconducting junctions. [25] We further assume the superconducting gap is larger than the excitonic one $\Gamma < \Delta$ and injection energy is smaller than superconducting gap: $\mathcal{E} < \Delta$. For zero incidence angle, in these limit we can strongly approximate the values of the momenta in the three regions:

$$\kappa_{\pm} \approx \sqrt{\frac{m}{\hbar^2}} \left(\sqrt{2G} \pm \frac{\mathcal{E}}{\sqrt{2G}} \right) = K_0 \pm K_{\mathcal{E}} \quad (25a)$$

$$q_{\pm} \approx \sqrt{\frac{m}{\hbar^2}} \left(\sqrt{2G} \pm \sqrt{\frac{\mathcal{E}^2 - \Gamma^2}{2G}} \right) = K_0 \pm K_{\Gamma} \quad (25b)$$

$$k_{\pm} \approx \sqrt{\frac{m}{\hbar^2}} \left(\sqrt{2G} \pm i \sqrt{\frac{\Delta^2 - \mathcal{E}^2}{2G}} \right) = K_0 \pm iK_{\Delta} \quad (25c)$$

For this choice of the energy scale, the coherent function of the superconductor lead $u_{T/B}$ and $v_{T/B}$ are complex

conjugates, thus we need to carry information of only one of them $v_{T/B} = u_{T/B}^*$ where only u_T is relevant. Whereas in the EC region we need to keep track of all of them but we can simplify the notation into $u_e = u_h = u$ and $v_e = v_h = v$. We find the coefficients for the components of EC wave function (14) by solving the boundary problem as first at $x = 0$ and at $x = L$, we then impose the equality of the coefficients obtained by at the two different boundaries. By combining all of these we obtain the following sets of equations for the reflection and transmission amplitudes:

$$\begin{aligned} & t_{\text{QET}} 2K_0 u u_T + t_{\text{QHT}} (K_{\Gamma} + iK_{\Delta}) u u_T^* - t_{\text{QEB}} (K_{\Gamma} + iK_{\Delta}) v u_T - t_{\text{QHB}} 2K_0 v u_T^* = \\ & e^{iq_+ L} [2K_0 u + r_{\text{NTT}} (K_{\Gamma} - K_{\mathcal{E}}) u - r_{\text{NTB}} 2K_0 u^*], \\ & t_{\text{QET}} (-iK_{\Delta} + K_{\Gamma}) u u_T + t_{\text{QHT}} 2K_0 u u_T^* - t_{\text{QEB}} 2K_0 v u_T - t_{\text{QHB}} (-iK_{\Delta} + K_{\Gamma}) v u_T^* = \\ & e^{-iq_+ L} [(K_{\Gamma} - K_{\mathcal{E}}) u + r_{\text{NTT}} 2K_0 u - r_{\text{NTB}} (K_{\Gamma} + K_{\mathcal{E}}) v], \\ & t_{\text{QET}} (iK_{\Delta} + K_{\Gamma}) v u_T - t_{\text{QHT}} 2K_0 v u_T^* + t_{\text{QEB}} 2K_0 u u_T - t_{\text{QHB}} (iK_{\Delta} + K_{\Gamma}) u u_T^* = \\ & e^{-iq_- L} [(K_{\Gamma} + K_{\mathcal{E}}) v - r_{\text{NTT}} 2K_0 v - r_{\text{NTB}} (K_{\Gamma} - K_{\mathcal{E}}) u], \\ & t_{\text{QET}} 2K_0 v u_T - t_{\text{QHT}} (K_{\Gamma} - iK_{\Delta}) v u_T^* + t_{\text{QEB}} (K_{\Gamma} - iK_{\Delta}) u u_T - t_{\text{QHB}} 2K_0 u u_T^* = \\ & -e^{iq_- L} [-2K_0 v + r_{\text{NTT}} v (K_{\mathcal{E}} + K_{\Gamma}) + r_{\text{NTB}} 2K_0 u], \\ & t_{\text{QET}} 2K_0 v u_T^* + t_{\text{QHT}} (K_{\Gamma} + iK_{\Delta}) v u_T - t_{\text{QEB}} (K_{\Gamma} + iK_{\Delta}) u u_T^* - t_{\text{QHB}} 2K_0 u u_T = \\ & -e^{iq_+ L} [(K_{\Gamma} - K_{\mathcal{E}}) u r_{\text{ATB}} - 2K_0 v r_{\text{ATT}}], \\ & t_{\text{QET}} (-iK_{\Delta} + K_{\Gamma}) v u_T^* + t_{\text{QHT}} 2K_0 v u_T - t_{\text{QEB}} 2K_0 u u_T^* - t_{\text{QHB}} (-iK_{\Delta} + K_{\Gamma}) u u_T = \\ & -e^{-iq_+ L} [2K_0 u r_{\text{ATB}} - (K_{\Gamma} + K_{\mathcal{E}}) v r_{\text{ATT}}], \\ & t_{\text{QET}} (iK_{\Delta} + K_{\Gamma}) u u_T^* - t_{\text{QHT}} 2K_0 u u_T + t_{\text{QHB}} 2K_0 v u_T^* - t_{\text{QHB}} (iK_{\Delta} + K_{\Gamma}) v u_T = \\ & -e^{-iq_- L} [(-K_{\Gamma} + K_{\mathcal{E}}) u r_{\text{ATT}} - 2K_0 v r_{\text{ATB}}], \\ & t_{\text{QET}} 2K_0 u u_T^* + t_{\text{QEB}} (-K_{\Gamma} + iK_{\Delta}) u u_T - t_{\text{QEB}} (-K_{\Gamma} + iK_{\Delta}) u^* u_T^* - t_{\text{QHB}} 2K_0 v u_T = \\ & e^{iq_- L} [(K_{\Gamma} + K_{\mathcal{E}}) v r_{\text{ATB}} + 2K_0 u r_{\text{ATT}}]. \end{aligned}$$

We can solve these eight equations with respect to the 4 reflections and transmissions amplitudes we obtain:

$$\begin{aligned} r_{\text{ATT}} &= \frac{4 (\text{Im}[u^2])^2 |u_T|^2}{u_T^2 (u^{*4} e^{-2\delta} + u^4 e^{2\delta}) - |u|^4 (u_T^{*2} 4 \sinh^2 \delta + 2u_T^2)} \\ &= \frac{a^2 \sqrt{1+b^2}}{[-a^2 \cosh(2\delta) - ab \sinh(2\delta)] + i[2b \sinh^2(\delta) + a \sinh(2\delta) - ba^2]} \end{aligned} \quad (26a)$$

and

$$\begin{aligned} r_{\text{NTB}} &= \frac{2 \sinh(\delta) |u|^2 \left[u^2 (u_T^{*2} e^{-\delta} + u_T^2 e^{\delta}) - u^{*2} (u_T^2 e^{-\delta} + u_T^{*2} e^{\delta}) \right]}{u_T^2 (u^{*4} e^{-2\delta} + u^4 e^{2\delta}) - |u|^4 (u_T^{*2} 4 \sinh^2 \delta + 2u_T^2)} \\ &= \frac{4 \sinh(\delta) |u|^2 i [a \cosh \delta + b \sinh \delta]}{[-a^2 \cosh(2\delta) - ab \sinh(2\delta)] + i[2b \sinh^2(\delta) + a \sinh(2\delta) - ba^2]}, \end{aligned} \quad (26b)$$

where in Eqs. (26a) and (26b) we have introduced $a = \sqrt{\Gamma^2 - \mathcal{E}^2}/\mathcal{E}$ and $b = \sqrt{\Delta^2 - \mathcal{E}^2}/\mathcal{E}$, the constant $\delta = L\xi_{\Gamma}$

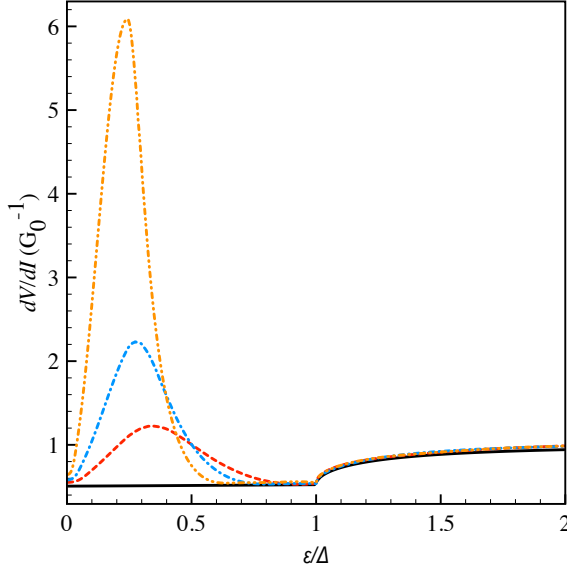


FIG. 6: Differential resistance as a function of the applied bias and different length of the EC region. In the figure we have set $\Gamma = 1$, $\Delta = 12\Gamma$, $G = 60\Gamma$ and $H_{\text{SM/EC}} = H_{\text{EC/SSM}} = 0.5$. The parameters are chosen in accord to Ref. [9, 31]. The different lines refer to $L = 0$ (black-solid line), $L = \xi_r/2$ (red dashed line), $L = 0.7\xi_r$ (blue dashed-dotted line), and $L = \xi_r$ (orange dashed-dashed-dotted line).

has been introduced in the main text. The other two reflection amplitudes r_{NTT} and r_{ATB} are smaller than the two in Eqs. (26) by an order $1/\sqrt{2G}$ and thus negligible, further, for energies smaller than the superconducting gap Δ the transmission probabilities are zero.

If we consider the limit of a long junction $\delta \gg 1$ we find that $r_{\text{ATT}} \rightarrow 0$ and $r_{\text{NTB}} \rightarrow 1$, exactly as we have found for the full numerical problem in the main text (c.f. Fig. 2 main text).

Case of HgTe quantum wells

The experiment by Kononov *et al.*, [9] explored the transport properties of a hybrid junction consisting of a

HgTe quantum well (QW) with a width of circa 20 nm. From previous studies, the authors know that the system is a indirect SM, with a small bands overlap. [31] This makes HgTe QWs candidates for observing a direct EC phase. Specifically in the experiment of Ref. [9], the QW is sandwiched between a normal and a superconductor contact. The transport measurements showed a zero bias anomaly in the differential resistance with an energy size comparable with the estimated EC gap of the system. [9]

We can use the results presented in the main text in order to explain the zero bias anomaly of the hybrid SM/EC/S junction. Assuming that the momentum displacement between the conduction and the valence band is small enough to be negligible, we can evaluate the differential resistance so as explained in the main text. The actual values of the system parameters can be extracted by Refs. [9, 31] and have: $G = 3.0$ meV, $\Gamma = 0.05$ meV and $\Delta = 0.6$ meV, which should correspond to a (Nb/FeNb)/HgTe structure explored in Ref. [9], we have further set a finite transparency of the two interface barriers $H_L = H_R = 0.5$. [9] For these parameters value we have an EC coherence length of $\xi_r = 955$ nm.

The results for the differential resistance are shown in S-Fig. 6. The black solid line describes a SM/SSM junction ($L = 0$), and coincides with the well-known results of the BTK theory after integration over injection angle (main text). [30] It is important to note that $\Delta/G = 0.50$ and hence the differential resistance at zero voltage is not exactly equal to $0.5G_0^{-1}$, which would be the result obtain in the leading order when $\Delta/G \ll 1$. By increasing the length of the EC region we obtain peak in the differential resistance at energies smaller than Δ . This result resemble the experimental observations of Ref. [9] that has been attributed as a manifestation of the EC phase.

The experiment of Ref. [9] also shown features in the superconducting sub-gap conductance that resemble the multiple-Andreev reflections (MARS) processes in voltage biased Josephson junctions. [33]. In principle such sub-gap features are unexpected, since in the experiment by Kononov *et al.* [9] there is only one superconducting electrode. Our model is also done for an unique S-electrode and in a quasi-equilibrium situation and therefore cannot describe MARS-like processes.